Synthetic aperture ladar based on a MOPAW laser

Simon Turbide, Linda Marchese, Alain Bergeron, Louis Desbiens, Patrick Paradis

Simon Turbide, Linda Marchese, Alain Bergeron, Louis Desbiens, Patrick Paradis, "Synthetic aperture ladar based on a MOPAW laser," Proc. SPIE 10005, Earth Resources and Environmental Remote Sensing/GIS Applications VII, 1000502 (18 October 2016); doi: 10.1117/12.2242232

Event: SPIE Remote Sensing, 2016, Edinburgh, United Kingdom

Synthetic aperture ladar based on a MOPAW laser

Simon Turbide, Linda Marchese, Alain Bergeron, Louis Desbiens and Patrick Paradis
INO, 2740 Einstein, Québec, Québec, Canada, G1P 4S4

ABSTRACT

Long range land surveillance is a critical need in numerous military and civilian security applications, such as threat detection, terrain mapping and disaster prevention. A key technology for land surveillance, synthetic aperture radar (SAR) continues to provide high resolution radar images in all weather conditions from remote distances. State of the art SAR systems based on dual-use satellites are capable of providing ground resolutions of one meter; while their airborne counterparts obtain resolutions of 10 cm.

Certain land surveillance applications such as subsidence monitoring, landslide hazard prediction and tactical target tracking could benefit from improved resolution. The ultimate limitation to the achievable resolution of any imaging system is its wavelength. State-of-the-art SAR systems are approaching this limit. The natural extension to improve resolution is to thus decrease the wavelength, i.e. design a synthetic aperture system in a different wavelength regime. One such system offering the potential for vastly improved resolution is Synthetic Aperture Ladar (SAL). This system operates at infrared wavelengths, ten thousand times smaller radar wavelengths.

This paper presents a SAL platform based on the INO Master Oscillator with Programmable Amplitude Waveform (MOPAW) laser that has a wavelength sweep of $\Delta\lambda$=1.22 nm, a pulse repetition rate up to 1 kHz and up to 200 µJ per pulse. The results for SAL 2D imagery at a range of 10 m are presented, indicating a reflectance sensibility of 8 %, ground-range and azimuth resolution of 1.7 mm and 0.84 mm respectively.

Keywords: Synthetic aperture ladar, synthetic aperture lidar, SAL, MOPAW

1. INTRODUCTION

Synthetic Aperture Radar (SAR) is a mature technology that overcomes the diffraction limit of an imaging system's real aperture by taking advantage of the platform motion to coherently sample multiple sections of an aperture much larger than the physical one. The backscattered data returns are then coherently reconstructed to produce the final high resolution SAR image. SAR has a significant history, the first experimental validation being carried out in 1953 at the University of Illinois [1]. This technology [2] has long been a valuable tool allowing high spatial resolution on both space-borne and airborne platforms, without the need for inconveniently large real apertures.

Synthetic Aperture Ladar (SAL) is the extension of SAR to much shorter wavelengths (1.5 µm vs 5 cm). This new technology [3][4][5] can offer higher resolution images in day or night time as well as in certain adverse conditions. It could be a powerful tool for Earth monitoring such as land surveillance applications from aircraft, unattended aerial vehicle (UAV) or spatial platforms. SAL could also be used as a complement to SAR: obtain a larger area coverage with SAR and deploy a SAL platform over the zone of interest to obtain higher resolution 2D or 3D images. The 3D SAL version based on phase difference is denoted by Interferometric SAL (IFSAL or InSAL).

Over the last decade, studies from different groups have been performed to validate the feasibility of a SAL system for 2D imagery[3][4][5] and more recently for 3D static target imagery [6]. One difficulty while developing a SAL system is the source which must provide a long linear sweep (for the range resolution), a high pulse repetition rate (in order to operate in realistic surveillance applications) and a high power density (for a minimal signal to noise ratio and a minimal ground coverage). This paper presents a SAL platform based on the INO Master Oscillator with Programmable Amplitude Waveform (MOPAW) laser which provides a good compromise between the different criteria.

Earth Resources and Environmental Remote Sensing/GIS Applications VII, edited by Ulrich Michel, Karsten Schulz, Manfred Ehlers, Konstantinos G. Nikolakopoulos, Daniel Civco, Proc. of SPIE Vol. 10005, 1000502
 · doi: 10.1117/12.2242232

2. SYNTHETIC APERTURE LADAR CONCEPT

2.1 SAL 2D acquisition and processing

In the most popular operation mode, strip map, an optical beam points along a fixed direction with respect to the flight platform path. A series of phase-encoded pulses illuminates the ground surface to cover a strip as the platform moves, as illustrated in Figure 1. The antenna pointing direction θ is different from zero to avoid confusion between the left and right side of the platform. The most commonly used pulse has a linear FM characteristic:

$$E(t) \propto \operatorname{rect}\left(\frac{t}{\tau}\right)\cos\left(2\pi f_0 t + \pi K t^2\right) \tag{1}$$

where τ is the pulse duration, f_0 is the instantaneous frequency at t=0 and K is the chirp rate. The electromagnetic field diffused from a point target of area δA_l on ground and collected by the bi-static configuration shown in Figure **1** is approximated by:

$$\begin{aligned} E_r(t,x) \propto \frac{1}{R_l(x)H_l(x)}\sqrt{\frac{A_0 P \delta A_l \rho_l}{\varphi_{beam-GR}\varphi_{beam-Az}}}\eta_H\left(x-x_l,y_l\right)w(x-x_l,y_l)\operatorname{rect}\left(\frac{t-\left(R_l(x)+H_l(x)\right)/c}{\tau}\right) \\ \cos\left(2\pi f_0(t-\left(R_l(x)+H_l(x)\right)/c)+\pi K(t-\left(R_l(x)+H_l(x)\right)/c)^2\right) \end{aligned} \tag{2}$$

where x represents the azimuth position of the platform and (x_l, y_l) are the ground-coordinates of the scatterer, ρ_l represents the scatterer`s reflectance and P is the beam power. The optical collection area is denoted by A_0, w is the normalized beam profile on ground and η_H is the collection efficiency of the diffused signal. $\varphi_{beam-GR}$ is the beam divergence in the ground-range (Y) direction while $\varphi_{beam-Az}$ is the beam divergence in the azimuth (X) direction. The transmitter-to-scatterer distance R_l is a function of the azimuth position, i.e $R_l = R_l(x-x_l)$, and similarly for the receiver-to-scatterer distance H_l. The platform moves in the azimuth direction with a constant velocity v.

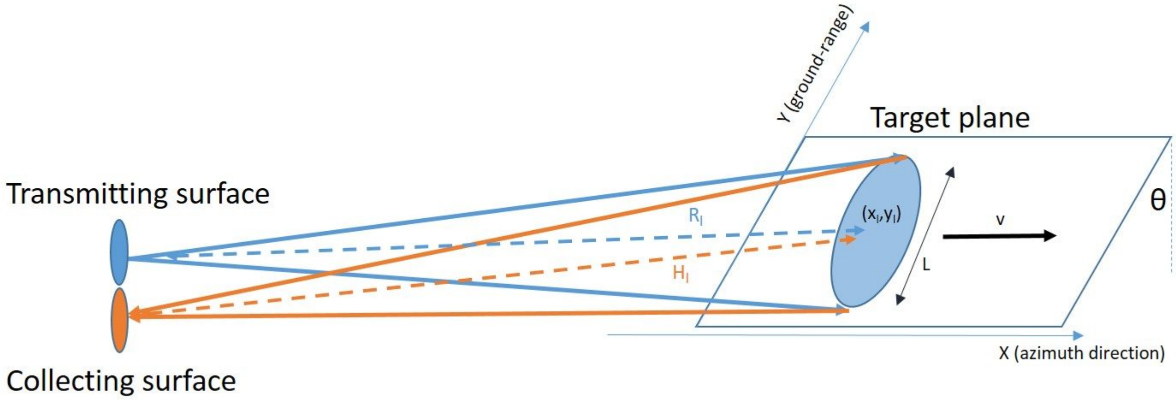

Figure 1: Bi-static SAL configuration with an elliptical beam.

The received signal E_r is demodulated before sampling by the mixing with a copy of the delayed pulse. The SAL raw data can be represented by the following complex signal

$$
\begin{aligned}
S_{SAL-raw}(t,x) \propto \sum_l \frac{1}{R_l(x)H_l(x)} \sqrt{\frac{A_0 P \delta A_l \rho_l}{\varphi_{beam-GR}\varphi_{beam-Az}}} \\
\eta_H(x-x_l, y_l) w(x-x_l, y_l) \mathrm{rect}\left(\frac{t-\left(R_l(x)+H_l(x)\right)/c}{\tau} \right) \\
\exp\left(i\frac{4\pi f_0}{c}\left(R_{ref}-\left(R_l(x)+H_l(x)\right)/2\right) + i\frac{4\pi K}{c}\left[R_{ref}-\left(R_l(x)+H_l(x)\right)/2\right]t \right)
\end{aligned}
\tag{3}
$$

where R_{ref} is the delayed pulse (the local oscillator) path length. The contribution from all scatterers on the ground is coherently added. Synthetic aperture raw data constitute a 2-D matrices block: the range dimension (the time t within a pulse emission) and the azimuth dimension (corresponding to different pulse emissions and represented by the platform position x). After digital (such as the Range –Doppler algorithm [2][7]) or optronic [8][9][10] processing, the SAL 2D image is given by:

$$
\begin{aligned}
I_{SAL-2D}(f_t,x) \propto \sum_l \frac{1}{R_l H_l} \sqrt{\frac{A_0 P \delta A_l \rho_l}{\varphi_{beam-GR}\varphi_{beam-Az}}} \exp\left(-i\frac{2\pi f_0\left(R_l+H_l\right)}{c} \right) \\
\mathrm{sinc}\left(\pi\tau\left[f_t - 2\frac{K}{c}(R_{ref}-\left(R_l+H_l\right)/2) \right] \right) P_w(x-x_l, y_l)
\end{aligned}
\tag{4}
$$

where f_t is the range frequency, P_w (a sinc-like function) is the Fourier transform (in azimuth) of $\eta_H w$ and (R_l, H_l) are the range of closest approach for the ground scatterer l. The ground-range and azimuth resolutions in the processed image are evaluated respectively from the sinc and from the P_w functions:

$$
\begin{aligned}
\delta y &\approx \frac{c}{2B_0 \sin\theta} \\
\delta x &\approx \frac{\lambda}{2\varphi_{beam-Az}}
\end{aligned}
\tag{5}
$$

where $\lambda = c/f_0$ is the center wavelength. The SAL resolution parameters are range independent. The main issue is therefore to have sufficient power density on target, as the range increase, to obtain an image with a sufficiently high SNR for the given spatial resolutions.

For a given beam footprint L in the ground-range direction, the intra-pulse sampling must satisfy Nyquist criterion, which lead to the minimal sampling rate:

$$
f \geq \frac{4KL\sin\theta}{c} \tag{6}
$$

3. DESCRIPTION OF THE SAL PLATFORM

3.1 The source

The INO SAL platform is based on a MOPAW Laser [11] which allow a good compromise between pulse repetition rate, energy per pulse and wavelength sweep. The key advantages of MOPAW systems lies in their ability to control the pulse generation and the optical amplification independently. INO introduced the tailoring of nanosecond pulse format in MOPAW fiber lasers around 1998, to produce rectangular optical pulses. Since then, the technology has evolved to provide more power, additional wavelengths, spatial beam modulation and an extended range of pulse durations. The previous MOPAW version allowed duration ranging from 1 ns to 1 µs. In order to enhance the beam coverage while keeping the sampling rate as low as possible, the MOPAW software was updated to allow a pulse duration up to 16 µs (we use a 4 µs pulse duration for the SAL application). This enhanced pulse duration reduced the chirp rate K for a given wavelength sweep.

For the application covered in this paper, the seed is a 1550 nm Distributed Feedback (DFB) diode. The wavelength modulation is a consequence of the current flowing in the seed: the linearity of the wavelength sweep was therefore adjusted by tuning the waveform amplitude (i.e. the current injected in the seed). This tuning was made automatically via MATAB: the seed output was sent to an interferometer with a fixed delay between the two paths and the waveform amplitude was iteratively adjusted to minimize the spectral distribution resulting from the signal Fast-Fourier transform. The pulse was adjusted with a temporal resolution of 1 ns and using 8192 levels for the amplitude control.

The shaped optical pulse is thereafter sent to a two-stage amplifier.. Target output pulse energies that keep the system within safe operating boundaries are calculated for each fiber amplifier stage.

The amplified signal is lastly coupled to a 1550 nm PM single-mode fiber, from which the main signal and the local oscillator are extracted (from a 99/1 splitter). The measured energy per pulse of the main signal is about 200 µJ for a pulse repetition rate of 1 kHz.

The temporal profile of the amplified signal is shown in the left panel of Figure 2. The section in red indicates the part used for the SAL application (the signal is truncated to that section in post-processing). The right panel of the figure shows the spectral distribution of the fixed-delay interferometer normalized output signal. The normalization consists into the division of the signal by the reference signal shown in the left panel. This normalization improves the spectral resolution. The range broadening correction method from Ref. [4] is finally applied. This broadening correction scheme turns out to have a negligible impact on the spectral width, which highlight the performance of the sweep linearization procedure described above. The wavelength sweep (calibrated with a HCN cell) is shown in Figure 3, along with a linear fit. The evaluated sweep range is $\Delta\lambda$=1.22 nm, which leads to a projected ground-range resolution of 1.7 mm.

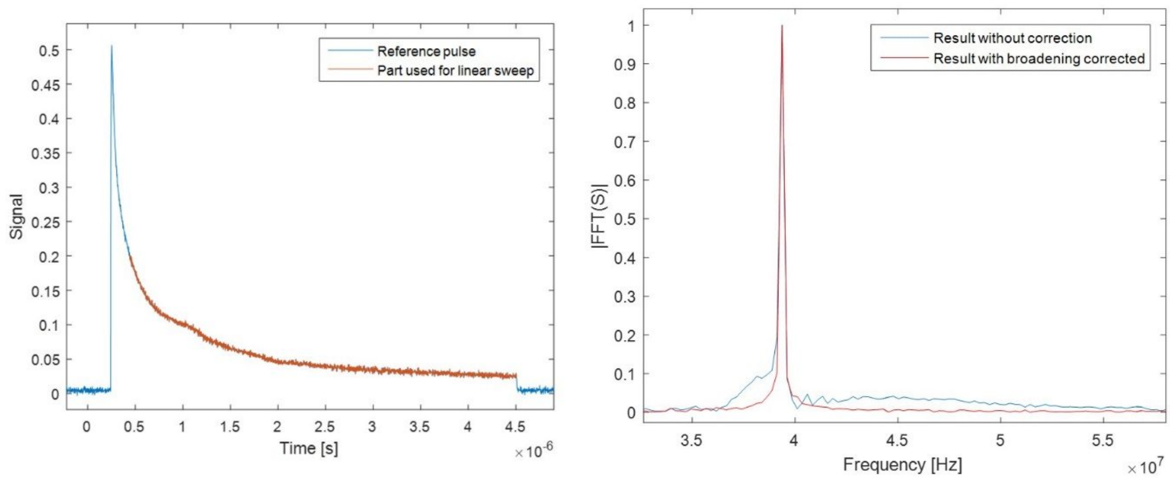

Figure 2: (Left panel) Pulse temporal signal after amplification. The red signal represents the part used for the linear sweep. (Right panel) Spectral distribution obtained by the FFT of the normalized output signal coming out of the fixed delay interferometer.

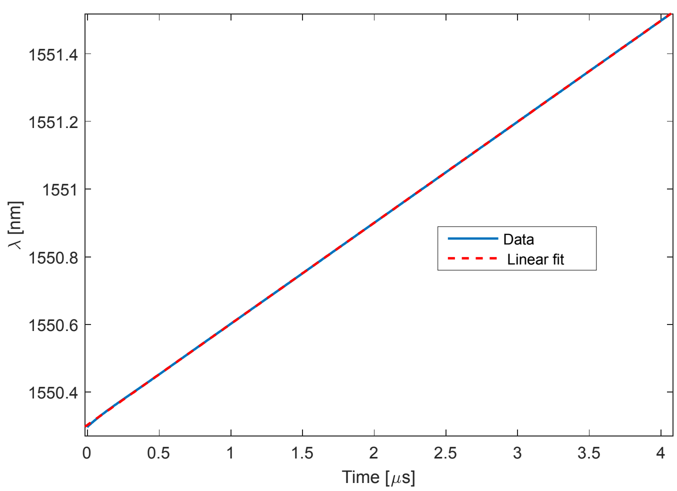

Figure 3: The measured wavelength sweep. The dashed line represents a linear fit.

3.2 The optomechanics

A picture of the optomechanics assembly is shown in Figure 4. A bi-static configuration is used: the bottom plate includes the optical elements for beam transmission while the top plate includes the elements for the diffused signal reception. Each plate includes a two lens set (a spherical lens and a cylindrical lens). The signal is emitted and collected with single mode PM optical fibers. The axial distances between the fiber ends and the lenses are adjustable to accommodate different beam footprints as a function of the range to target. The cylindrical lens makes the beam elliptical: the beam divergence is higher in the across-track direction than in the azimuth direction. This ellipse shape maximizes the ground-coverage, at the expense of some azimuth resolution loss [12]. An image of the beam footprint (in a plane transverse to beam propagation) at a range of 3 m is shown in Figure 5. The beam dimension at this range is about 14 x 3.3 cm, the short axis being in the azimuth direction. The beam dimension in the target plane is therefore 19.8 x 3.3 cm. The azimuth beam divergence is $\varphi_{beam\text{-}Az} = 11$ mrad. The stretch factor (the long axis divide by the short axis) is therefore 4.3 for this example. The stretch factor can be modified by changing the distance between the two lenses. In order to maximize the signal collection, the same distance adjustment (between fiber and first lens and between the two lenses) is made with the reception board.

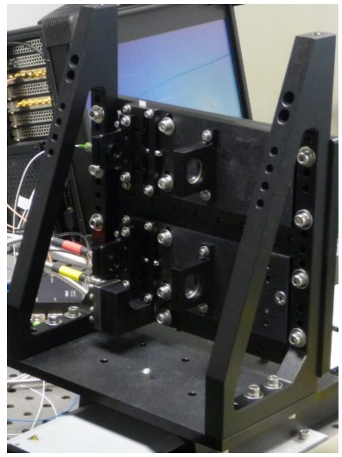

Figure 4: The optomechanics assembly used for the SAL platform. It represents a bi-static configuration: the bottom plate includes the optical elements for beam transmission while the top plate includes the optical elements for the signal collection.

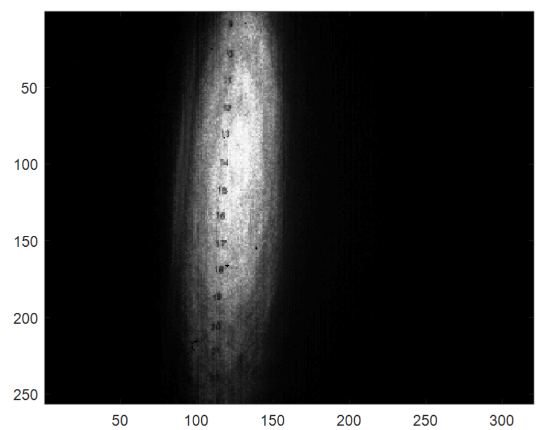

Figure 5: Beam footprint at a range of 3 m. The image of the laser beam diffusion from a white paper sheet is measured with a Xenics BOBCAT camera. The vertical graduation (along the beam long range axis) is in cm.

3.3 SAL measurement procedure

A picture of the SAL setup is shown in Figure 6. The two black boxes at the front is the MOPAW assembly. At the back, we see the optomechanics which sits over the translation stage (PI, model M-521-DD). To obtain a SAL image, the pulse repetition rate is set at 1 kHz, the target plane is inclined by 45 deg. relatively to the beam propagation and the stage translation speed is set to 5 mm/s, which leads to a Δx=5 µm displacement in between two pulses. The Nyquist criterion for the azimuth sampling is [1]:

$$\Delta x_{\max} \geq \frac{\lambda}{2\varphi_{beam-Az}} \tag{7}$$

which gives Δx_{max}=70 µm. The platform velocity could in principle be increased up to 7 cm/s while satisfying the Nyquist criterion. However, by using a slower speed than necessary, we obtain more traces that are then incoherently added (Multilook processing [1]) to improve the image SNR. For the results presented in the next section, 10 000 traces were recorded for each image.

The delay of the local oscillator was adjusted (via optical fiber patch cord) to the range to target back and forth distance. The signal collected by the reception fiber was mixed with the local oscillator (with a 50/50 optical fiber coupler) before detection with a 200 MHz bandwidth balanced detector (Thorlabs, model PDB460 C). The signal is finally sampled at a rate of 750 MHz, with the 12 Bit GageScope shown in the picture. The beginning of each trace follows the trigger provided by the MOPAW. The control of the laser, the translation stage, the data sampling and the data transfer (from the on-board acquisition memory to the Hard disk) are managed with a LabVIEW program.

In postprocessing, using Matlab, each trace was truncated to the optimum part shown in Figure 2 and normalized by the reference signal profile to improve the spectral resolution. Finally, the range-Doppler algorithm was applied to obtain the 2D images.

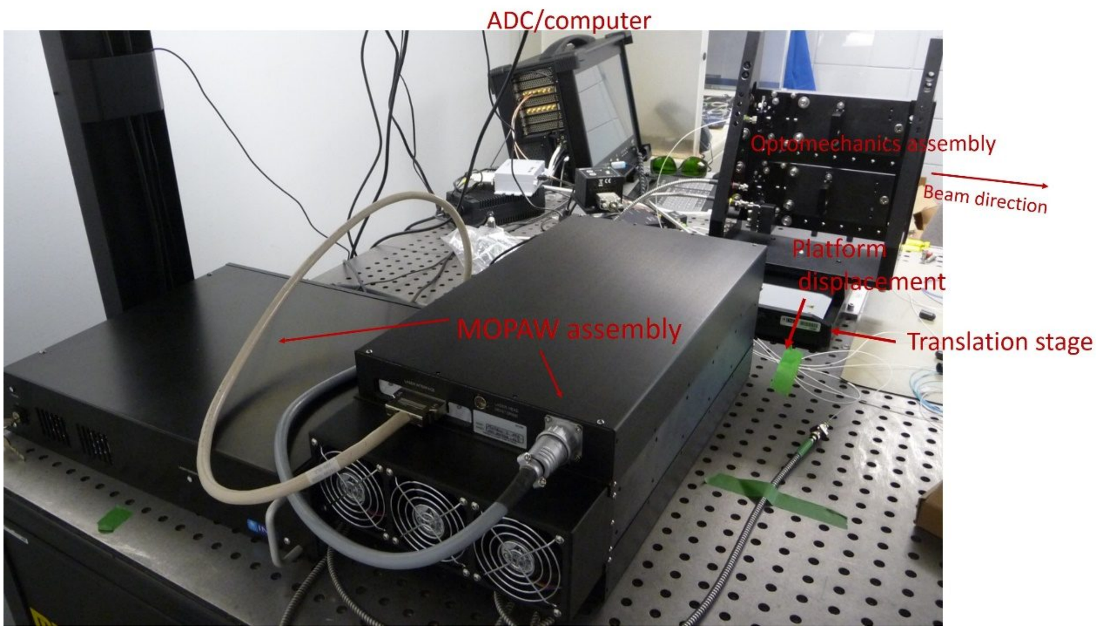

Figure 6: Picture of the SAL setup

4. SAL RESULTS

The tests were done with an 'INO' target with a strip above, all made of white paper. A picture of the target is shown in the left panel of Figure 7. The target dimension was about 3.5 x 6 cm. The first SAL measurement was done at a range of 1.23 m with all lenses removed from the optomechanics setup, in order to valided the system in its simplest configuration. The corresponding SAL image is shown in the right panel of Figure 7. In spite of the speckles (which is inherent to all Synthetic Aperture images), the INO target is clearly visible, with however a slightly different orientation of the letters, due to a small tilt of the target plane (i.e. a tilt of the target X dimension relatively to the platform direction).

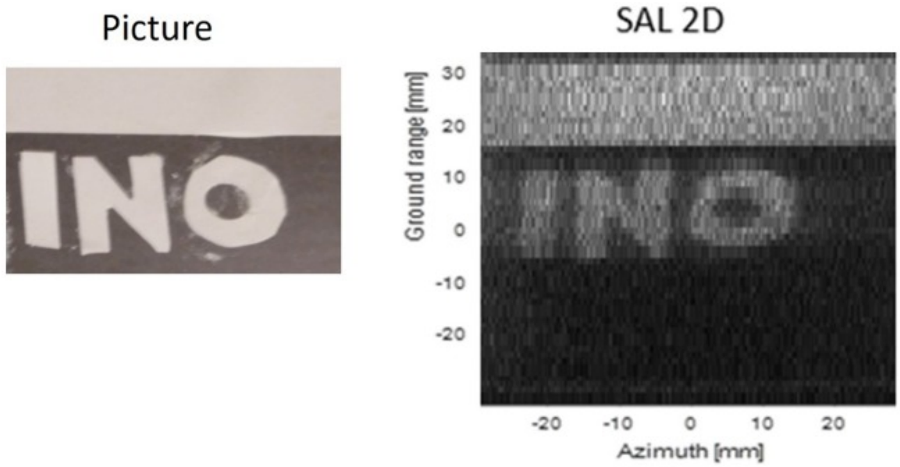

Figure 7: Picture of the target used for test (left panel) and the corresponding SAL image (right panel) for a 1.23 m range without optics.

The SAL image of the target at a range of 3 m is shown in Figure 8, this time including all optical elements leading to the ellipse shaped footprint shown in Figure 5. The image point-target (a 4 mm ball lens) is apparent at the top of the image. This ball lens (see the picture in Figure 9) was introduced to validate the image focused and evaluated the azimuth resolution. The azimuth profile of the ball lens is shown in Figure 10, from which the resolution (the Full Width at Half Maximum) is evaluated to 0.87 mm. The theoretical azimuth resolution, from Eq. (5) and taking into account the azimuth resolution loss due to the Multilook processing, is about 0.2 mm, indicating a residual defocus in the image.

The signal to noise ratio (SNR) of the 'INO' image is about 55. Since the reflectance of the white paper sheet is about ρ=70 % [13] and because the SAL image depends on $\sqrt{\rho}$, we evaluated the reflectance sensitivity on the SAL image to be about 5 %. This sensitivity was evaluated as the variation of reflectance leading to an intensity variation, in the image, equal to two times the noise level. Finally, a line of sight image of the target at 3 m, as seen from just behind the optomechanics assembly, is shown in Figure 11.

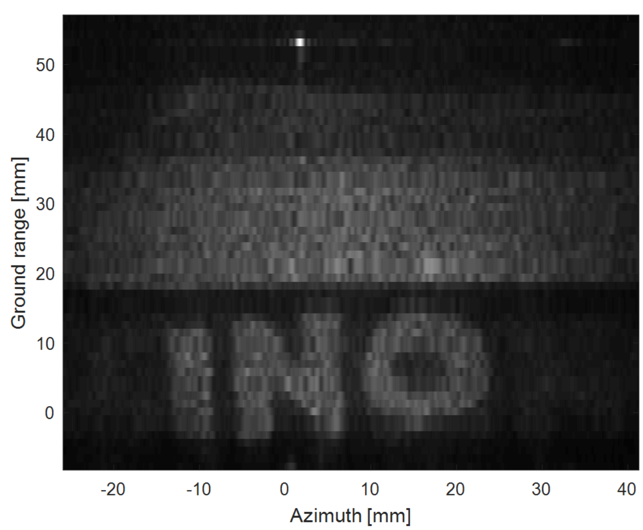

Figure 8: SAL image of the INO target and the ball lens, for a range of 3 m.

Figure 9: Picture of the 4 mm ball lens used to test the azimuth focusing.

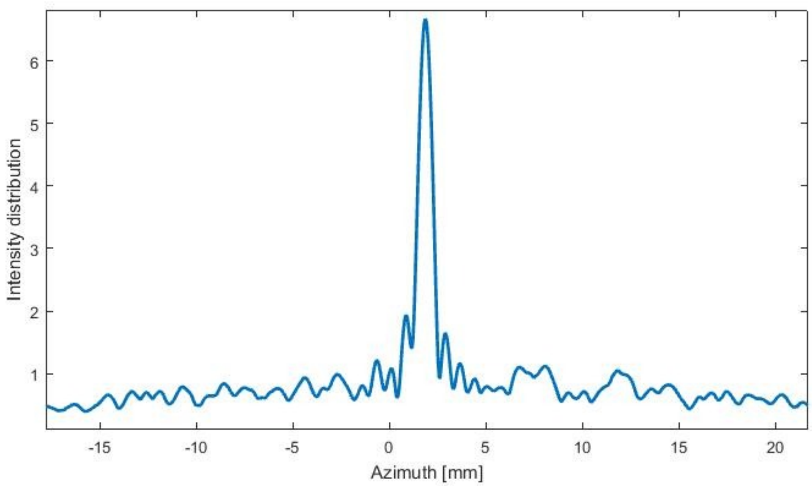

Figure 10: Azimuth distribution of the ball lens SAL image, for a range of 3 m.

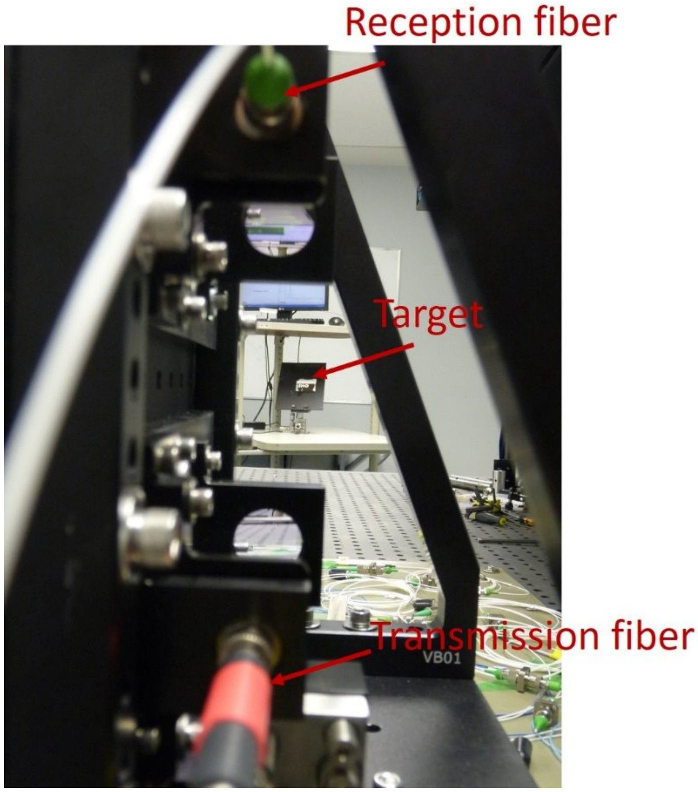

Figure 11: Line of sight picture of the target as seen from behind the optomechanics assembly, for a range of 3 m.

After this laboratory demonstration, the SAL platform was set on a trolley to test at longer range. A picture of the rapidly deployable SAL platform is shown in the left panel of Figure 12. The right panel shows the line of sight view of the target at a 10 m range, along the INO basement corridor. The resulting SAL image is shown in Figure 13. The beam footprint in the target plane for this configuration was about 42 cm x 8.6 cm. The SNR of the 'INO' image at 10 m is about 38, the azimuth resolution is 0.84 mm and the reflectance sensibility is 8 %. Finally, a SAL image of a black anodized aluminum plate is shown in Figure 14. Although the reflectance of the black finish plate is weak, the shape of the plate and the (non-adonized) holes are clearly visible in the SAL image.

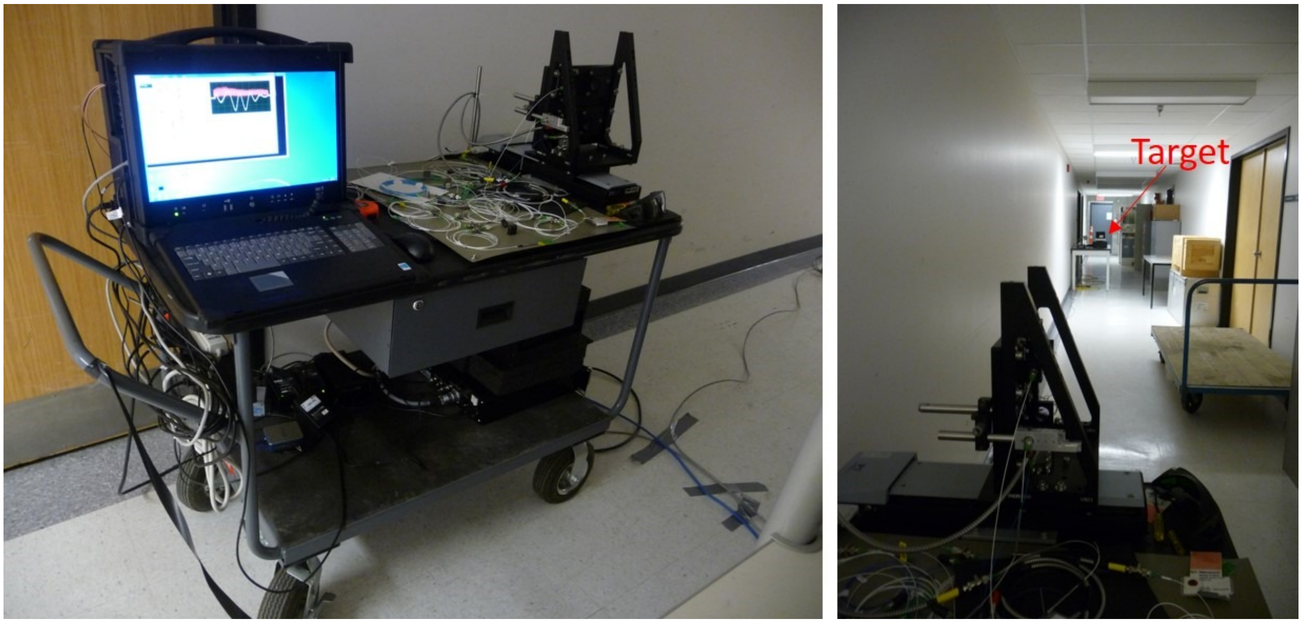

Figure 12: The deployable SAL platform is shown in the left panel. The line of sight picture of the target at a range of 10 m is shown on the right panel.

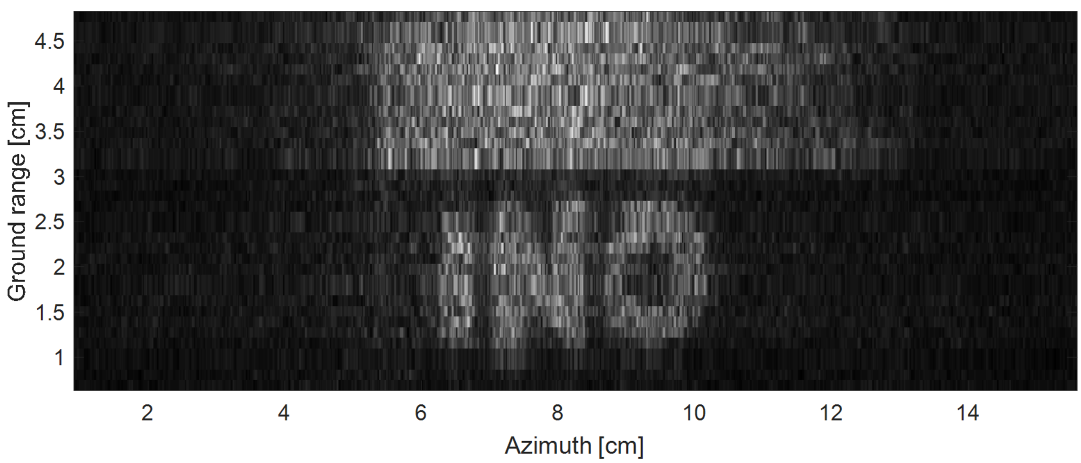

Figure 13: SAL image of the INO target at a range of 10 m.

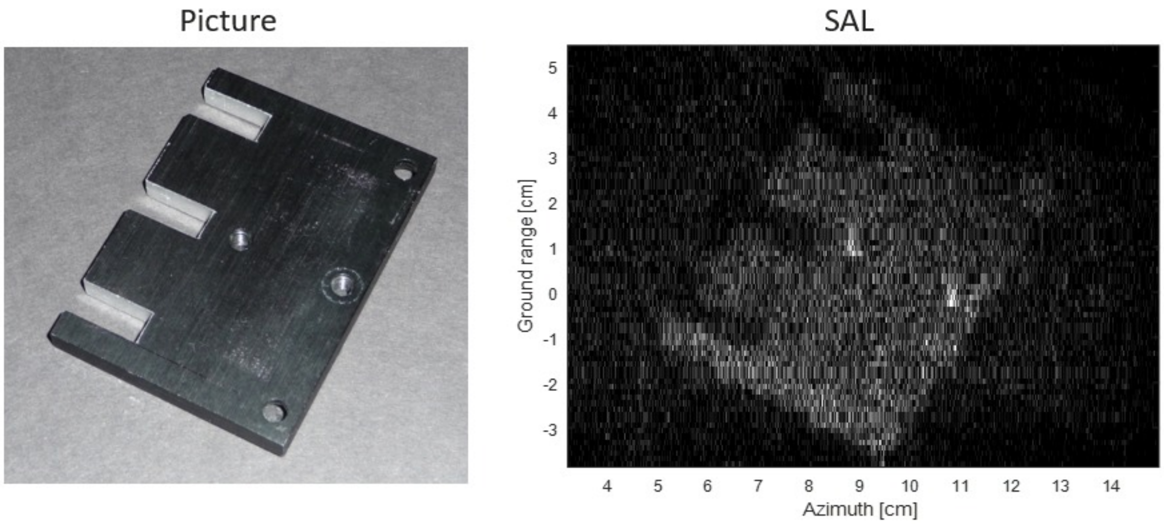

Figure 14: Picture of black anodized aluminum plate (left panel) and the corresponding SAL image (right panel).

5. CONCLUSIONS

A SAL platform based on the INO Mopaw laser has been presented in this paper. The SAL-Mopaw uses a DFB diode seed at 1550 nm. The wavelength sweep is a consequence of the current flowing in the seed: the linearity of the wavelength sweep was adjusted by tuning the current amplitude. The performance of this tuning is such that a subsequent range broadening correction is unnecessary. The platform is based on 4 µs pulses emitted at a rate of 1 kHz and the energy per pulse is 200 µJ. A bi-static configuration, with a two-lenses set for the transmitter and the receptor, was used. The two-lenses set included a cylindrical lens to produce a beam footprint with an ellipse shape. This shape allows for an enhanced ground-coverage at the expense of some azimuthal resolution loss.

Results for 2D SAL imagery were presented for different ranges, from 1.23 m to 10 m. The ground-range and azimuth resolution were evaluated to be 1.7 mm and 0.84mm respectively, while the reflectance sensibility was evaluated to be 5 % at a range of 3m and 8% at a range of 10m. Test at longer range (up to 50 m) will be done soon outdoor with that platform. Thanks to the flexibility of the optomechanics configuration, the ellipse shape stretch factor will be increased further to improve the power density on the target plane in order reduced the invserse square law effect on the image intensity. These future tests with the INO SAL platform, with its mm resolution and cm/s displacement speed, should show its potential for surveillance applications.

REFERENCES

[1] G. Franceschetti and R. Lanari, *Synthetic aperture radar processing*, CRC Press, (1999).

[2] J.C. Curlander and R.N. McDonough, *Synthetic Aperture Radar: systems and Signal Processing*, John Wiley & Sons, Inc., New York, (1991).

[3] M. Bashkansky, R. L. Lucke, E. Funk, L. J.Rickard, and J. Reintjes, *Two-dimensional synthetic aperture imaging in the optical domain*, Opt. Lett. **27**, 1983 (2003).

[4] S. M. Beck, j. R. Buck, W. F. Buell, R. P. Dickinson, D. A. Dozlowski, N. J. Marechal, and T. J. Wright, *Synthetic aperture imaging laser radar: laboratory demonstration and signal processing*, Appl. Opt. **44**, 7621 (2005).

[5] W. Buell, N. Marechal, J. Buck, et al., *Demonstration of synthetic aperture imaging ladar*, Proc. Of SPIE, Vol. 5791, 152 (2005).

[6] S. Crouch and Z.W. Barber, *Laboratory demonstrations of interferometric and spotlight synthetic aperture ladar techniques*, Opt. Exp. **20**, 24237 (2012).

[7] I.G. Cumming and F.H. Wong, *Digital processing of synthetic aperture radar data: algorithms & implementation*, Artec House, Boston (2005).

[8] L. Marchese, M. Doucet, B. Harnish, M. Suess, P. Bourqui, M. Legros, N. Desnoyers, L. Guillot, L. Mercier, M. Savard, A. Martel, F. Chateauneuf, A Bergeron, *Ultra-Rapid optronic Processor for Instantaneous ENVISAT/ASAR Scene Observation*, IGARSS 2010, IEEE, Honolulu, HI, pp. 685-687, July (2010).

[9] A. Bergeron, M. Doucet, B. Harnish, M. Suess, L. Marchese, P. Bourqui, N. Desnoyers, M. Legros, L. Guillot, L. Mercier, F. Chateauneuf, *Satellite In-Board Real-Time SAR Processor Prototype*, ICSO 2010, IEEE, Rhodes, Greece, October (2010).

[10] L. Marchese, S. Turbide, M. Terroux and A. Bergeron, *All Optical Synthetic Aperture Lidar Sensing-To-Processing Chain Based on SAR Technology*, IGARSS, Munich, Germany, July (2012).

[11] L. Desbiens, P. Deladurantaye, A. Cournoyer, D. Gay, C. Paré, S. Eiselen, V. Roy and Y. Taillon, *Flexible and Programable Pulse Shapping MOPA Fiber Laser Platform, Performances and Applications*, Laser Review, Vol 41, No 9, (2013).

[12] S. Turbide, L. Marchese, M. Terroux and A. Bergeron, Investigation of Synthetic Aperture Ladar for Land Surveillance Applications, Proc. of SPIE 8897, no 889709, (2013).

[13] USGS Digital Spectral Library, http://speclab.cr.usgs.gov/spectral.lib06/ds231/datatable.html.